

Large Fluorescence Enhancement via Lossless All-Dielectric Spherical Mesocavities

Vadim I. Zakomirnyi,^{*,†} Alexander Moroz,[‡] Rohit Bhargava,[¶] and Ilia L. Rasskazov[§]

[†]*Beckman Institute for Advanced Science and Technology, University of Illinois at Urbana-Champaign, Urbana, IL 61801, USA*

[‡]*Wave-scattering.com*

[¶]*Departments of Bioengineering, Electrical & Computer Engineering, Mechanical Science & Engineering, Chemical and Biomolecular Engineering and Chemistry, Cancer Center at Illinois, Beckman Institute for Advanced Science and Technology, University of Illinois at Urbana-Champaign, Urbana, IL 61801, USA*

[§]*SunDensity Inc., Rochester, NY 14604, USA*

E-mail: vazak@illinois.edu

Abstract

Nano- and microparticles are popular media to enhance optical signals, including fluorescence from a dye proximal to the particle. Here we show that homogeneous, lossless, all-dielectric spheres with diameters in the mesoscale range, between nano- ($\lesssim 100$ nm) and micro- ($\gtrsim 1$ μ m) scales, can offer surprisingly large fluorescence enhancements, up to $F \sim 10^4$. With the absence of nonradiative Ohmic losses inherent to plasmonic particles, we show that F can increase, decrease or even stay the same with increasing intrinsic quantum yield q_0 , for suppressed, enhanced or intact radiative decay rates of a fluorophore, respectively. Further, the fluorophore may be located inside or outside the particle, providing additional flexibility and

opportunities to design fit for purpose particles. The presented analysis with simple dielectric spheres should spur further interest in this less-explored scale of particles and experimental investigations to realize their potential for applications in imaging, molecular sensing, light coupling, and quantum information processing.

Keywords: fluorescence, all-dielectric sphere, Mie theory, mesocavity, photonics

Introduction

Light-matter interactions are of fundamental importance for advances in a variety of fields, including information technology, sustainable energy, chemical sensing, and spectroscopy. In particular, extensive research has been driven by the quest to control the electromagnetic effects associated with light at the nanoscale over the past few decades. Plasmonic nanoparticles (NPs) made of noble (Au, Ag)¹ and post-transition (Al)^{2,3} metals, transparent conducting oxides (Al:ZnO, Ga:ZnO),^{4,5} and transition-metal nitrides (TiN, ZrN)^{5,6} are well-known to enhance the electromagnetic field on the nanoscale, enabling extraordinary opportunities for boosting various optical effects and for control over electromagnetic radiation in unusual ways. While immensely successful, the efficiency of optical devices based on plasmonic metal NPs is often limited due to the Joule, or Ohmic, losses associated with the (free) electron response of metals. Mitigation of these losses has persisted as a challenge and has spurred the search for alternatives. One such route is to use high-quality resonances within all-dielectric particles⁷ for all-dielectric photonics. One of the most exciting and well-developed applications of plasmonic and all-dielectric NPs have been *enhanced fluorescence*. Fluorescence underlies many modern detection modalities, especially molecularly-specific recognition of species in low abundance in biological systems. Since intrinsic fluorescence emission can be very weak, the development of high-performance devices can be challenging for important applications such as single molecule detection,^{8,9} sensitive early diagnostics,^{10–12} bioimaging,¹³ detection in complex food and drug safety backgrounds,¹⁴ fingerprint tags,¹⁵ advanced light sources, such as micro/nano light-emitting diodes (LEDs) for high-resolution displays,^{16,17} and single pho-

ton sources for quantum photonics.^{18,19} Here we address the problem of enhancing fluorescence in order to improve present possibilities and enable potentially promising applications.

Though large fields around plasmonic NPs are beneficial for fluorescence excitation, unavoidable Ohmic losses reduce the quantum yield. As all-dielectric particles do not suffer from these limiting losses, they are a potentially powerful avenue for fluorescence enhancement. However, as widely believed and revealed quantitatively in recent comparative studies,^{20,21} all-dielectric particles cannot enhance fluorescence in a manner comparable to plasmonic NPs due to the relatively smaller locally supported electric fields and, consequently, a low enhancement factor. Giant fluorescence enhancement factors reported, thus, are mostly based on a paradigm of *metal*-enhanced fluorescence (MEF), where the use of dielectrics is generally limited to acting as a spacer to keep an emitter at an optimal distance from a metal surface. With almost two decades of intensive development of MEF,²² the highest recorded fluorescence enhancement factor of 910 – 2300 is considered to be via Ag nanocubes,^{23,24} which may well be an upper bound of MEF for single particles since Ag is the most favorable plasmonic material for near-field enhancement.^{25,26} Although Mie theory²⁷ has been known for more than a century, rising interest in resonant optical properties of all-dielectric nanostructures has been triggered by recent advances in the fabrication of individual dielectric particles with a controlled geometry.⁷ The resonant behavior of high-index (GaAs, Si, Ge, TiO₂) particles enables realization of low-loss nonplasmonic metamaterials and metasurfaces with rich optical functionalities, along with enhanced light–matter interactions and advanced linear and nonlinear light manipulations. Despite an impressive number of obvious advantages of all-dielectric particles, the relatively weaker electric field enhancement compared to plasmonic NPs is widely considered to represent their major drawback, seemingly limiting their utilization.

Here we demonstrate that all-dielectric particles with sizes in an intermediate region between the nanoscale ($\lesssim 100$ nm) and microscale ($\gtrsim 1$ μ m), or the *mesoscale* region, are exceptionally suitable for fluorescence enhancements. The dominant prevalent approaches aim to keep particle sizes as small as possible (e.g. in nanometer range) while accessing higher order resonances. Alas,

this leads to conflicting requirements. If the particle size becomes too small, higher order multipole resonances cannot be accessed in the common excitation wavelength ranges for fluorescent species. When particle sizes become too large, in contrast, whispering gallery mode resonances start to dominate that result in extremely small line widths.^{28,29} Such particles also become too large for many applications due to steric limitations. By focusing on the mesoscale region, we sought to achieve a compromise between nano- and microworlds while being able to combine the advantages of the both. Our design hypothesis was that mesocavities (MCs) can allow us access to intermediary multipolar resonances ($4 \lesssim l \lesssim 10$) in the visible and near-infrared wavelength ranges. These resonances are well below the typical order of whispering gallery modes ($l \gtrsim 20$) in microparticles;^{28,29} however, their quality factors are much higher than of the orders ($l \lesssim 2$) that can be accessed by nanoparticles. Such mesoparticles can possess resonances with a quality factor up to $\approx 10^4$ compared to a quality factor of ≈ 20 for a typical dipole resonance within a plasmonic NP. In this manuscript, we use results of our fast numerical open source code Stratify³⁰ to design and study mesoscale particles and to gain insight into their optical responses with a view to optimize their structure and realize their potential for enhancing fluorescence.

Results and Discussion

Consider a fluorescence emitter as an oscillating electric dipole (ED).^{31–36} The enhanced fluorescence can be described in two steps as shown in Figure 1. In this model, first, a particle locally

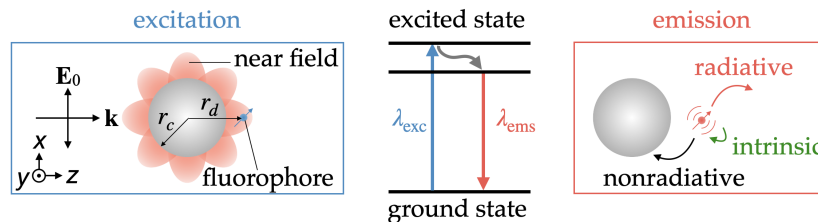


Figure 1: Conventional two-level model for a particle enhanced fluorescence: excitation process under a plane wave illumination and emission process with ED radiation.

enhances an electric field, E_{loc} . This, in turn, amplifies the excitation rate, $\gamma_{exc} (\propto |E_{loc}|^2)$, of the

emitter. Second, after being excited, the mutual interaction with the particle modifies the radiative decay rate, Γ_{rad} , of the dipole emitter. The presence of dissipative components also induces changes in the nonradiative decay rate, Γ_{nrad} . Contrary to the widespread misconception that fluorescence enhancement is proportional to radiative decay enhancement, the resulting fluorescence enhancement factor is determined by^{20,34,37,38}

$$F = \frac{\gamma_{\text{exc}}}{\gamma_{\text{exc};0}} \frac{q}{q_0} = \frac{\gamma_{\text{exc}}}{\gamma_{\text{exc};0}} \frac{\tilde{\Gamma}_{\text{rad}}}{\tilde{\Gamma}_{\text{rad}} + \tilde{\Gamma}_{\text{nrad}} + (1 - q_0)/q_0} \frac{1}{q_0}, \quad (1)$$

where the subscript “0” indicates the respective quantity in the free space, the rates with tilde are normalized to the *radiative* decay rate in free space (e.g. $\tilde{\Gamma}_{\text{rad}} = \Gamma_{\text{rad}}/\Gamma_{\text{rad};0}$, $\tilde{\Gamma}_{\text{nrad}} = \Gamma_{\text{nrad}}/\Gamma_{\text{rad};0}$), and q_0 is the intrinsic quantum yield. $\tilde{\Gamma}_{\text{rad}}$, which corresponds to the radiative decay enhancement, is determined by the local density of states, whereas $\tilde{\Gamma}_{\text{nrad}}$ is determined by particle losses. In the special case of $q_0 = 1$ and $\tilde{\Gamma}_{\text{nrad}} = 0$, the last two fractions on the rhs of eq 1 reduce to unity. Any fluorescence enhancement is then determined solely by the first fraction, i.e. by the excitation enhancement, and the fluorescence enhancement in the above particular case is insensitive to any local density of states (LDOS) changes at the emission wavelength. The above illustrates that fluorescence enhancement is a more complex process than radiative decay enhancement and that one should avoid any temptation to characterize fluorescence by either the LDOS or the Purcell factor.

The fluorescence excitation and emission processes are treated independently (i.e., weak coupling) and, in general, there is a Stokes shift between excitation, λ_{exc} , and emission, λ_{ems} , wavelengths, i.e. $\Delta\lambda_s = \lambda_{\text{ems}} - \lambda_{\text{exc}} \neq 0$. The emitter is assumed to be below saturation.^{37,39} According to eq 1, achieving an optimal fluorescence enhancement factor requires a delicate balance of γ_{exc} on one hand, and of $\tilde{\Gamma}_{\text{rad}}$ and $\tilde{\Gamma}_{\text{nrad}}$ on the other hand.^{37,39–43}

Light-matter interaction of a generic process involving an ED characterized by its ED moment \mathbf{d} is proportional to $\sim \mathbf{E} \cdot \mathbf{d}$. Excitation rates are then proportional to $|\mathbf{E} \cdot \mathbf{d}|^2$. In order to facilitate ensuing calculations, the following common averaging over the ED orientation and its position on

a spherical shell of fixed radius r are performed (see Supporting Information for details):

- the ED moment \mathbf{d} in the scalar product $|\mathbf{E} \cdot \mathbf{d}|^2$ is averaged over all possible orientations of \mathbf{d} at a given fixed \mathbf{r} , whereby $|\mathbf{E} \cdot \mathbf{d}|^2$ reduces to $\frac{1}{3}|\mathbf{E}|^2|\mathbf{d}|^2$
- after averaging over all possible orientations of \mathbf{d} at a given fixed \mathbf{r} , the resulting scalar product $\frac{1}{3}|\mathbf{E}|^2|\mathbf{d}|^2$ is averaged over the spherical surface of fixed radius r .

As a result of this averaging, it is possible to reformulate the scalar product into the respective averages of $|\mathbf{E}|^2$ and $|\mathbf{d}|^2$.³⁷ After the above averaging, the excitation rate, $\gamma = |\mathbf{E} \cdot \mathbf{d}|^2$, becomes proportional to the surface averaged intensity of the electric field, $\bar{\gamma} \propto \oint |\mathbf{E}|^2 d\mathbf{S}$. The latter can be determined by closed-form analytical formulas of ref 44. The averaged $\bar{\gamma}$ is obviously r -dependent and does not depend on the spherical angular coordinates. The corresponding decay rates become orientation averaged decay rates^{36,37} after the above averaging, $\Gamma_{(n)\text{rad}} = (\Gamma_{(n)\text{rad}}^\perp + 2\Gamma_{(n)\text{rad}}^\parallel)/3$, where superscripts “ \perp ” and “ \parallel ” denote the radial and tangential orientations of ED, respectively. All the above steps are implemented in freely available MATLAB code, Stratify,³⁰ employed in the present simulations. In essence, surface integrals of the electric field intensity can be performed analytically and *the calculation of average intensity costs the same computational time as determining intensity at a given single point*. This strategy allows simulating potentially promising designs at a low computational cost, without the need for time-expensive calculations of electric fields at multiple points inside or outside a particle. Once configurations of MCs exhibiting large *averaged* values of $|\mathbf{E}_{\text{loc}}|^2$ are identified, further detailed calculations of electric fields for these designs are easily implemented (cf. Figure 3).

The rich modal composition of high-index MCs necessitates a delicate search for suitable resonances. This optimization can be complicated to accomplish as both optimal electric field localization and decay rates need to be optimized for fluorescence enhancement, eq 1. The complexity of this problem is a key challenge why previous works^{20,21} did not find the utility of all-dielectric particles for fluorescence enhancement.

The *averaged* fluorescence enhancement factor (eq 1) in the presence of a lossless ($\tilde{\Gamma}_{\text{nrad}} = 0$)

all-dielectric particle reduces to

$$\bar{F} = \frac{\tilde{\gamma}_{\text{exc}}}{\tilde{\gamma}_{\text{exc};0}} \frac{\tilde{\Gamma}_{\text{rad}}}{1 - q_0 + q_0 \tilde{\Gamma}_{\text{rad}}}. \quad (2)$$

To relate to practical applications, we consider widely used and readily fabricated TiO_2 spherical particles with real refractive index $n_c = 2.7$, which are lossless in the visible range,⁷ and vary their radii from 10 to 500 nm, thus sampling both the “nano” (radii from 10 to 50 nm) and “meso” regimes (radii from 50 to 500 nm). For the sake of illustration, either standard Nile Blue dye with $\lambda_{\text{exc}} = 633$ nm and $\lambda_{\text{ems}} = 663$ nm, or Er^{3+} with $\lambda_{\text{exc}} = 488$ nm and $\lambda_{\text{ems}} = 1530$ nm is used as ED emitter. It is also worth noting that modern fabrication techniques can embed emitters into spheres with nanometer precision in the radial direction for a number of different materials.^{45,46} Controlled positioning of emitters outside the sphere is possible by attaching emitters to (nano)particles via molecular techniques, such as using single-stranded DNA (ssDNA) spacers⁴⁷ or DNA origami.⁴⁸ Therefore, we consider situations with an emitter both inside and outside of a TiO_2 sphere. Figures 2(a-c) show excitation and radiative decay rates for two different ED orientations. Extinction spectra for the transverse electric (TE), also called magnetic, and transverse magnetic (TM), also called electric, modes are superimposed on the top of the graphs to show the nature of resonances. The peaks in the radiative decay rate correlate nicely with the peaks in the modes having dominant electric field components along the ED direction, i.e. the TE (TM) mode for the tangential (radial) ED orientation.

Similar to our previous study,⁴⁹ we observe that it is more beneficial to tune a suitable resonance to an emitter excitation wavelength than to its emission wavelength for enhancing \bar{F} . This is because an enhancement in $\tilde{\Gamma}_{\text{rad}}$ does not need to have any effect on enhancing fluorescence. In view of eq 2, \bar{F} is proportional to $\tilde{\Gamma}_{\text{rad}}$ only for intrinsic quantum yield $q_0 \equiv 0$, whereas \bar{F} is independent of $\tilde{\Gamma}_{\text{rad}}$ for $q_0 = 1$.⁵⁰

Tuning a suitable *magnetic* (TE) MC resonance to the excitation wavelength was found to be the most beneficial. The so-called decay rate engineering advocated within the MEF framework as

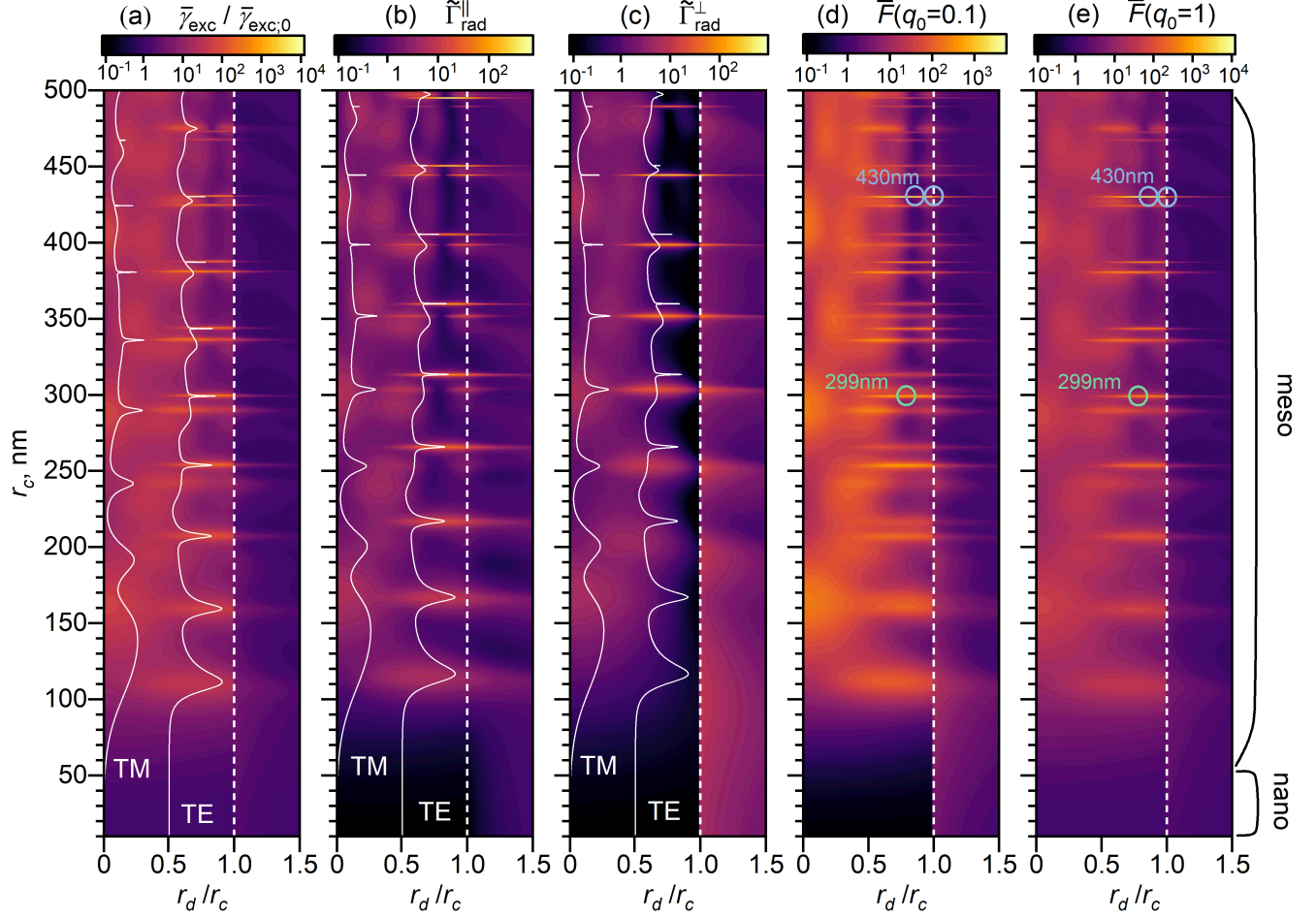


Figure 2: Maps of different quantities as a function of sphere radius, r_c , on the y-axis and relative ED radial position, r_d/r_c , on the x-axis for TiO_2 MC in the air: (a) Averaged excitation rate enhancement. (b)-(c) Normalized radiative decay rate for ED with the respective (b) tangential and (c) radial orientation. (d)-(e) Respective averaged fluorescence enhancement \bar{F} for ED with quantum yield (d) $q_0 = 0.1$ and (e) $q_0 = 1$. Dashed vertical lines at $r_d/r_c = 1$ in all plots denote the sphere surface. Curves in (a)-(c) show normalized extinction of corresponding TiO_2 spheres decomposed into the transverse electric (TE) and transverse magnetic (TM) (with horizontal offset for clarity) modes at $\lambda_{\text{exc}} = 633$ nm in (a) and at $\lambda_{\text{ems}} = 663$ nm in (b), (c). The peaks in the radiative decay rate correlate nicely with the peaks in the modes having dominant electric field components along the ED direction, i.e. the TE (TM) mode for the tangential (radial) ED orientation. Circles in (d) and (e) correspond to configurations considered in detail in Figures 3 and 4.

means of enhancing $F^{22,51}$ plays a smaller role in the present case of MCs.

In the interstitial case described by the virtual-cavity model,⁵² the local field, \mathbf{E}_{loc} , felt by

emitters *inside* the particle in the presence of a macroscopic field \mathbf{E} is $\mathbf{E}_{\text{loc}} = L_{\text{vc}}\mathbf{E}$, where

$$L_{\text{vc}} = \frac{n_c^2 + 2}{3} \quad (3)$$

is the so-called Lorentz local-field correction⁵² (see Supporting Information for its general derivation from the Maxwell's equations). This correction is particularly interesting for high-index dielectrics because L_{vc} linearly increases with the host dielectric constant, and it can become large. Averaged fluorescence enhancements \bar{F} displayed in Figures 2(d),(e) for ED for two different values of q_0 (0.1 and 1) are shown with the Lorentz local-field correction included (contributing for $n_c = 2.7$ the factor of $L_{\text{vc}}^2 \approx 9.6$ to $\bar{\gamma}_{\text{exc}}$).

Figure 3a,b shows extinction efficiency and normalized intensity of the electric field, $|\mathbf{E}_{\text{loc}}|^2/|\mathbf{E}_0|^2$ (at λ_{exc}), inside and outside TiO_2 sphere with radius (a) $r_c = 430$ nm and (b) $r_c = 299$ nm, on the background of the respective TE and TM resonances. The results correspond to the incident plane-wave amplitude \mathbf{E}_0 oscillating along the x axis and propagation along the z axis, as indicated in Figure 1.

Local fields enhancement demonstrates rarely studied patterns of $l = 8$ and $l = 5$ multipoles induced in MCs with $r_c = 430$ nm and $r_c = 299$ nm, respectively. We notice that optimal arrangement of emitters into hot spots of a mesosphere can further increase the ultimate fluorescence enhancement factor. Interestingly, the spatial extent of these hot spots is quite broad, which makes them suitable for any application benefiting from strong electric field enhancement.

Coupling of ED to a dielectric mesoparticle can result in strong modification of angular emission of ED. To analyze it, we have calculated the radiation directivity (relation of the power emitted into a certain direction to the solid angle averaged emitted power) of ED in the vicinity of TiO_2 mesoparticle at $\lambda_{\text{ems}} = 663$ nm, which corresponds to the maximum of emission wavelength of Nile Blue dye. Figure 3(c)-(e) shows the angular directivity of radially (\perp) and tangentially (\parallel) oriented ED at specific relative positions highlighted in Figure 2. It can be seen that radially oriented ED doesn't have large directionality. Tangentially oriented ED, on the other hand, has

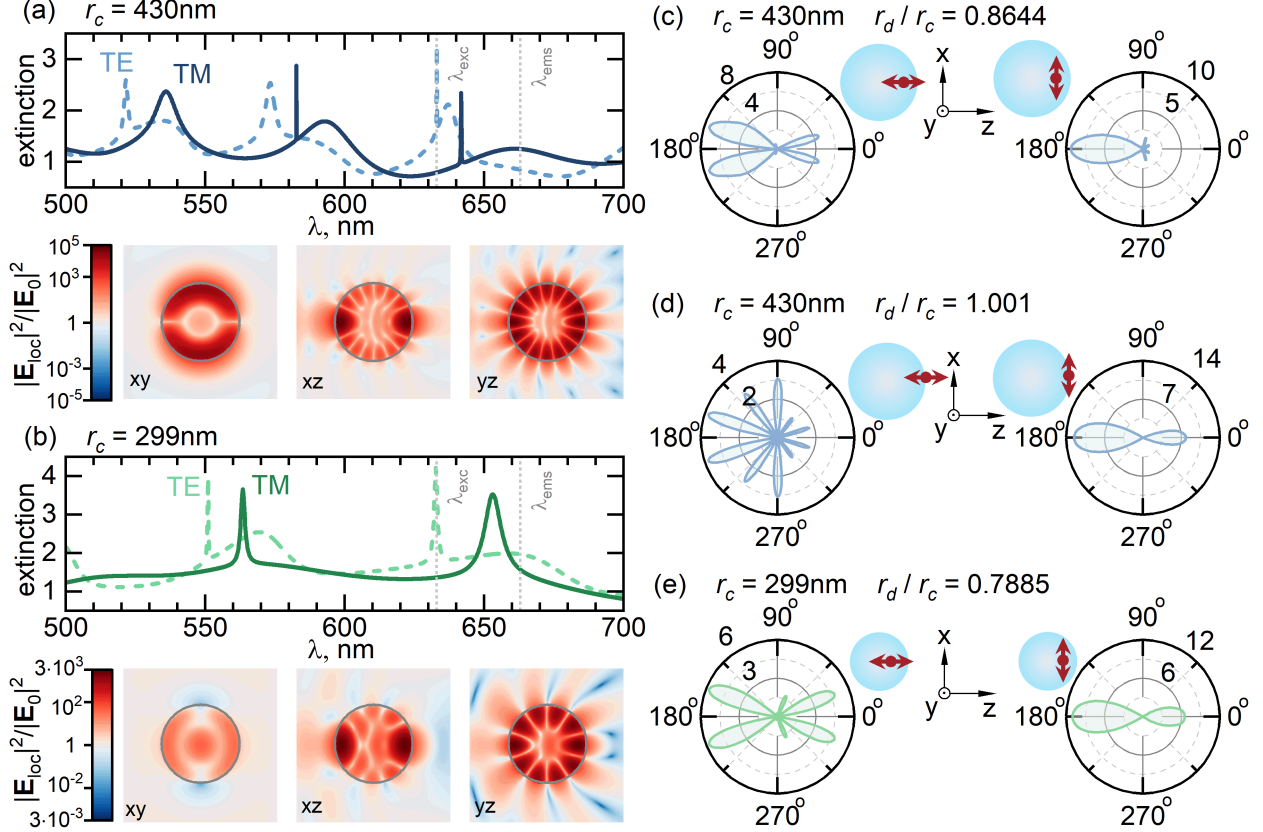


Figure 3: (a-b) Extinction efficiency decomposed into the transverse electric (TE) and transverse magnetic (TM) modes as a function of wavelength, and normalized intensity of the electric field, $|\mathbf{E}_{\text{loc}}|^2/|\mathbf{E}_0|^2$, at λ_{exc} inside and outside TiO_2 sphere with radius (a) $r_c = 430$ nm and (b) $r_c = 299$ nm. The results correspond to the incident plane-wave amplitude \mathbf{E}_0 oscillating along the x axis and propagation along the z axis as indicated in Figure 1. Vertical dashed lines in extinction spectra correspond to excitation and emission wavelengths of Nile Blue dye. (c)-(e) Polar plots (in the xz plane) of angle-resolved directivity (in dB) of ED emitting at $\lambda_{\text{ems}} = 663$ nm for its radial (left – along the z axis) and tangential (right – along the x axis) orientations. The following sizes of MC and relative radial positions of the ED are considered (cf. Figure 2): (c) $r_c = 430$ nm, $r_d/r_c = 0.8644$ (d) $r_c = 430$ nm, $r_d/r_c = 1.001$ and (e) $r_c = 299$ nm, $r_d/r_c = 0.7885$. The directivity varies with the angle θ , being oriented to the free space for $\theta = 0^\circ$ and toward the center of the particle for $\theta = 180^\circ$.

a highly directional pattern of emission oriented toward mesoparticle ($\theta = 180^\circ$). Interestingly, ≈ 12 directivity for ED with tangential orientation embedded inside the mesoparticle with 299 nm (Figure 3(e)) approaches the fundamental Harrington-Chu limit^{53,54} (≈ 13.69 for a given sphere size and λ_{ems}).

If in the lossless case described by eq 2: (i) $\tilde{\Gamma}_{\text{rad}} > 1$ then q/q_0 (the second fraction in eq 2) grows as q_0 decreases; (ii) $\tilde{\Gamma}_{\text{rad}} < 1$ then q/q_0 grows as q_0 increases; (iii) $\tilde{\Gamma}_{\text{rad}} = 1$ then q/q_0

does not depend on q_0 . As shown in Figure 4, one can encounter all three cases in practice. Contrary to the case of plasmonic particles characterized by significant $\tilde{\Gamma}_{\text{nrad}}$ in their proximity

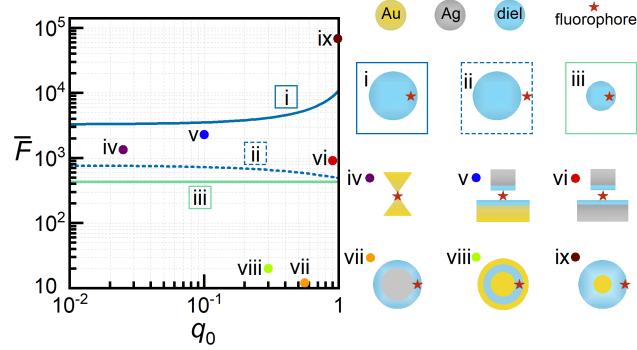


Figure 4: Averaged fluorescence enhancement as a function of q_0 for three different $\text{TiO}_2@$ Nile Blue configurations highlighted in Figure 2d,e: (i) $r_c = 430$ nm and $r_d/r_c = 0.8644$, (ii) $r_c = 430$ nm and $r_d/r_c = 1.001$, (iii) $r_c = 299$ nm and $r_d/r_c = 0.7885$. $\tilde{\Gamma}_{\text{nrad}} \equiv 0$ implies the absence of familiar $\bar{F} \sim 1/q_0$ scaling within the MEF framework.⁵⁰ For comparison, the most representative cases of fluorescence enhancements and respective q_0 described in previous studies are shown: (iv) bow-tie Au antenna,⁵⁵ (v) Ag nanocubes on Au film,²³ (vi) Ag nanocubes on Ag film,²⁴ (vii) Ag@dielectric core-shells,⁵⁶ (viii) Au@dielectric@Au matryoshkas,⁵⁷ (ix) Au@dielectric mesoscale core-shell⁴⁹ (the result therein has been multiplied by the factor of 22.56, which corresponds to L_{vc}^2 for the dielectric shell with $n_s = 3.5$ considered in ref 49). The comparison with other geometries is to illustrate the potential of our simple geometry at a different scale. In addition to the optimized geometries for each shape, an end user must also consider the constraints of the application to choose one of these options.

due to large Ohmic losses leading to a scaling $\bar{F} \sim 1/q_0$ behavior in q_0 ,⁵⁰ we have $\tilde{\Gamma}_{\text{nrad}} = 0$ here and, consequently, there is no scaling in q_0 . In fact, the maximum achievable \bar{F} can be increasing (i.e. not decreasing) with increasing q_0 as can be seen from Figure 4.

Enhancement mediated by dielectric nanoparticles is a common approach to increasing the intensity of fluorescence signals emitted by fluorescent molecules or materials. When fluorescent molecules are placed near dielectric nanoparticles or embedded in them, the nanoparticles can act as efficient scattering elements, increasing the excitation and/or emission rate of these fluorescent molecules through the enhanced local field effect. The choice between dielectric microparticles and nanoparticles for the purpose of fluorescence enhancement depends on the specific requirements of the application, such as the desired enhancement factor, the photostability of the fluorescent molecule, and compatibility with the experimental conditions. In our study, we show

that much larger fluorescence enhancement can be achieved with meso-sized particles than with nanoparticles. Contrary to earlier studies involving all-dielectric microparticles,^{28,29} our study has been strictly limited to particle sizes between nanoscale ($\lesssim 100$ nm) and microscale ($\gtrsim 1$ μ m) and, consequently, to intermediary multipolar resonances ($4 \lesssim l \lesssim 10$) that is well below typical order of whispering gallery modes ($l \gtrsim 20$) in microparticles. The present proposal seems to be an excellent compromise between nano- and microworlds while being able to combine the advantages of both worlds.

Recently, we have reported that a metal core is essential to get extraordinary fluorescence enhancements exceeding 3000 (results presented therein are shown without taking into account the local field corrections).⁴⁹ The reported fluorescence enhancement by homogeneous all-dielectric MCs is only slightly smaller than that reported in ref 49 (cf. Figure 4), while bringing significant manufacturing advantages: (i) homogeneous all-dielectric MC are generally much easier to fabricate, (ii) do not require costly noble metals, and (iii) allow one to embed emitters in their entire volume (or realize other options⁴⁵) potentially leading to brighter fluorescence sources. Dielectric MCs can provide a tunable and uniform enhancement effect over a wide range of wavelengths. This is because the resonant frequency of the dielectric MCs can be tailored to match the excitation and emission wavelengths of the fluorescent molecule, leading to a more efficient energy transfer.

We next discuss practical aspects of utilizing mesoparticles for fluorescence enhancement (Figure 5). We start with examining the effect of particle size polydispersity on the practically achievable fluorescence enhancements. Given that a typical full width at half maximum (fwhm) of organic dyes absorption band is at least 50 nm,^{58,59} and assuming as large as ± 5 nm range of particle size distribution about a target size, the latter size variations can be easily accommodated by a tunable laser diode source, enabling one to excite dyes on the particle resonance, while still remaining within a dye absorption band. Figure 5 shows that the effect of the particle size polydispersity under the above provisions is rather small. As a matter of fact, even as large as ± 20 nm range of particle size distribution about a target size would be sufficient for enjoying enhanced fluorescence for most applications. We have also observed another interesting result from this figure: high flu-

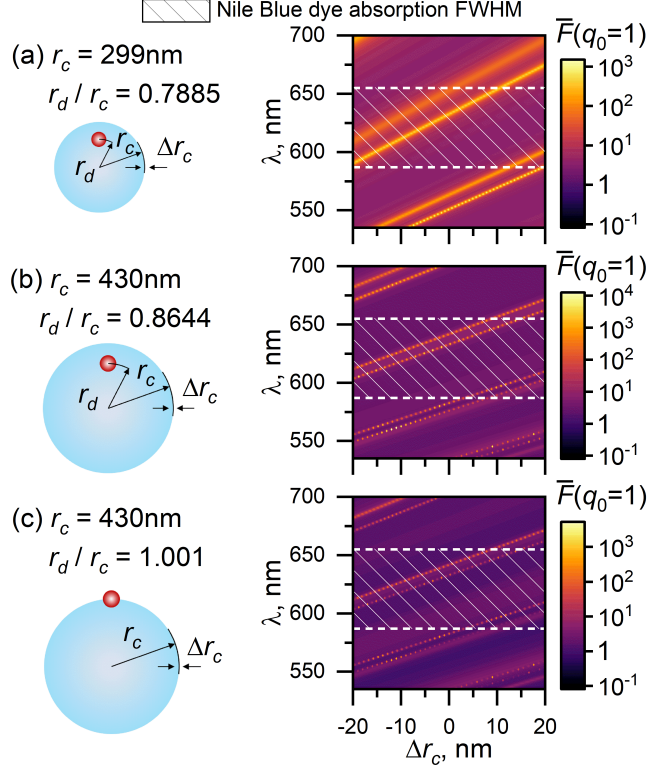


Figure 5: Averaged fluorescence enhancement \bar{F} as a function of wavelength and of the deviation, Δr_c , in the size of MC from optimally chosen (cf. Figure 2): (a) $r_c = 299$ nm, (b) $r_c = 430$ nm, and (c) $r_c = 430$ nm. As Δr_c varies excitation is assumed to be tuned to the corresponding resonance by a tunable (e.g. laser diode) source. Corresponding relative positions of ED are fixed to be the same for different Δr_c values and are denoted in the respective sketches. The shaded area between horizontal dashed lines in all plots denotes the fwhm of Nile Blue dye absorption spectra.

orescence enhancement values can be achieved for all possible values of Δr_c within the range of predefined r_c and r_d/r_c . This is enabled by the high multipole order of resonance of the particles, occurring at a wavelength that coincides with the maximum of fluorescence. It is clear that the shaded area between the horizontal dashed lines, which corresponds to the fwhm of the absorption spectrum of Nile Blue dye, will always be enhanced by the presence of 5th-8th order TE or TM resonances of dielectric MC.

While we have considered a single emitter thus far, other emitters and species may also be proximally present. Let us consider the effect of multiple emitters (Figure 6). Once an emitter is excited, it can transfer its excitation to a nearby emitter via an energy transfer mechanism. With multiple emitters present, this transfer process increases the probability of a decay of emitter ex-

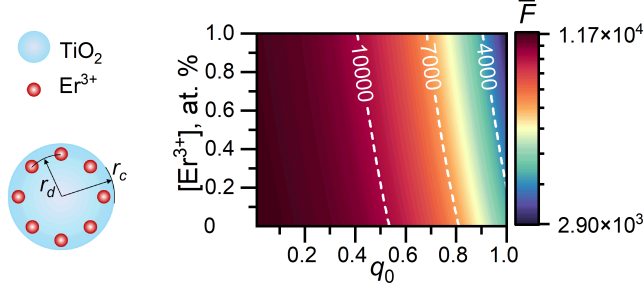


Figure 6: Averaged fluorescence enhancement \bar{F} for $\text{TiO}_2@\text{Er}^{3+}$ composites as a function of the Er^{3+} concentration and intrinsic quantum yield q_0 . TiO_2 sphere of radius $r_c = 489$ nm embedded in water ($n_h = 1.33$) with Er^{3+} emitters located at fixed $r_d = 438$ nm distance from the sphere center.

citation. Similarly, if the excitation is transferred to an emitter in a proximity of an impurity, the excitation can be quenched (e.g., OH bonds in silica), whereby the excitation disappears without ever contributing to radiation. This is the essence of the so-called concentration quenching, which does contribute to nonradiative decay rate but whose origin is different from the Ohmic losses of metal particles. In what follows, we consider Er^{3+} emitters with $\lambda_{\text{exc}} = 488$ nm and $\lambda_{\text{ems}} = 1530$ nm coupled to TiO_2 mesoparticle embedded in water with $n_h = 1.33$. Concentration quenching in this case can be accounted by⁶⁰

$$\Gamma_{\text{nrad}} = 8\pi C_{\text{Er-Er}}[\text{Er}^{3+}][Q], \quad (4)$$

where $[\text{Er}^{3+}]$ ($[Q]$) is the erbium (quencher) concentration in at. %, and $C_{\text{Er-Er}}$ is a coupling constant. Using a typical coupling value for $C_{\text{Er-Er}}$ from the literature ($10^{-39} \text{ cm}^6 \text{ s}^{-1}$), we also assume a quencher concentration of 100 ppm for representative calculations. For example, assuming the dominant quencher in SiO_2 is OH, this is a reasonable value for the colloids prepared in a wet-chemical reaction.⁶⁰ The effect of Er^{3+} concentration on the averaged fluorescence enhancement \bar{F} is highlighted in Figure 6. Interestingly, even relatively small nonradiative losses have the effect similar to that in the MEF,⁵⁰ namely larger \bar{F} are attainable with smaller q_0 . In the case of non-zero nonradiative losses, utilization of the emitters with the Stokes shift, $\Delta\lambda_s$, smaller than the resonance line width can be beneficial allowing one to achieve large $\bar{\gamma}_{\text{exc}}$ and $\bar{\Gamma}_{\text{rad}}$ simultaneously,

thus counteracting any emergent quenching induced by $\tilde{\Gamma}_{\text{rad}} \neq 0$.

Conclusions

By using our fast calculation approach, modeling showed that *size matters*: for a given sphere of specific refractive index, much larger fluorescence enhancement can be achieved with meso-sized homogeneous dielectric spheres than with nanospheres. Quite surprisingly, record high averaged fluorescence enhancements for all-dielectric particles of $\bar{F} \sim 10^4$ can be achieved with simple homogeneous mesospheres under optimal conditions without requiring the engineering of sophisticated shapes, precise nanogaps, generation of hot spots, or designer metasurfaces. Potential fluorescence enhancements are much larger than those obtained experimentally (Figure 4). Given the importance of fluorescence in numerous practical applications, we find it a very important result beneficial for fluorescence applications to imaging, sensing, strong coupling, and quantum information processing. Only averaged quantities have been discussed so far; it is to be expected that fluorescence enhancements of individual fluorophores can be a further magnitude larger if they are optimally arranged into hot spots of a mesosphere.

Methods

Numerical results reported in this manuscript have been obtained via open source code Stratify.^{30,61} Detailed derivations and the respective expressions for quantities entering master eq (2) are available as follows: $\bar{\gamma}_{\text{exc}}/\bar{\gamma}_{\text{exc};0}$ ^{44,62} and $\tilde{\Gamma}_{\text{rad}}$.^{31,33,36}

Supporting Information Available

Averaged fluorescence enhancement as a proper figure of merit. A general derivation of the Lorentz local-field correction directly from the Maxwell's equations.

Associated Content: Vadim I. Zakomirnyi; Alexander Moroz; Rohit Bhargava; Ilia L. Rasskazov. Large fluorescence enhancement via lossless all-dielectric spherical mesocavities. 2023. arXiv. <https://arxiv.org/abs/2301.10899> (accessed December 1, 2023)

References

1. Ostovar, B.; Cai, Y.-Y.; Tauzin, L. J.; Lee, S. A.; Ahmadvand, A.; Zhang, R.; Nordlander, P.; Link, S. Increased intraband transitions in smaller gold nanorods enhance light emission. *ACS Nano* **2020**, *14*, 15757–15765.
2. Knight, M. W.; King, N. S.; Liu, L.; Everitt, H. O.; Nordlander, P.; Halas, N. J. Aluminum for plasmonics. *ACS Nano* **2014**, *8*, 834–840.
3. Gérard, D.; Gray, S. K. Aluminium plasmonics. *Journal of Physics D: Applied Physics* **2015**, *48*, 184001.
4. West, P.; Ishii, S.; Naik, G.; Emani, N.; Shalaev, V.; Boltasseva, A. Searching for better plasmonic materials. *Laser & Photonics Reviews* **2010**, *4*, 795–808.
5. Naik, G. V.; Kim, J.; Boltasseva, A. Oxides and nitrides as alternative plasmonic materials in the optical range [Invited]. *Optical Materials Express* **2011**, *1*, 1090–1099.
6. Naik, G. V.; Schroeder, J. L.; Ni, X.; Kildishev, A. V.; Sands, T. D.; Boltasseva, A. Titanium nitride as a plasmonic material for visible and near-infrared wavelengths. *Optical Materials Express* **2012**, *2*, 478–489.
7. Baranov, D. G.; Zuev, D. A.; Lepeshov, S. I.; Kotov, O. V.; Krasnok, A. E.; Evlyukhin, A. B.; Chichkov, B. N. All-dielectric nanophotonics: the quest for better materials and fabrication techniques. *Optica* **2017**, *4*, 814–825.
8. Stehr, F.; Stein, J.; Schueder, F.; Schwille, P.; Jungmann, R. Flat-top TIRF illumination boosts DNA-PAINT imaging and quantification. *Nature Communications* **2019**, *10*, 1268.

9. Ray, S.; Widom, J. R.; Walter, N. G. Life under the microscope: Single-molecule fluorescence highlights the RNA world. *Chemical Reviews* **2018**, *118*, 4120–4155.
10. Bower, A. J.; Li, J.; Chaney, E. J.; Marjanovic, M.; Spillman, D. R.; Boppart, S. A. High-speed imaging of transient metabolic dynamics using two-photon fluorescence lifetime imaging microscopy. *Optica* **2018**, *5*, 1290–1296.
11. Garcia, M.; Edmiston, C.; York, T.; Marinov, R.; Mondal, S.; Zhu, N.; Sudlow, G. P.; Akers, W. J.; Margenthaler, J.; Achilefu, S.; Liang, R.; Zayed, M. A.; Pepino, M. Y.; Gruev, V. Bio-inspired imager improves sensitivity in near-infrared fluorescence image-guided surgery. *Optica* **2018**, *5*, 413–422.
12. Park, S.-J.; Kim, B.; Choi, S.; Balasubramaniam, S.; Lee, S.-C.; Lee, J. Y.; Kim, H. S.; Kim, J.-Y.; Kim, J.-J.; Lee, Y.-A.; Kang, N.-Y.; Kim, J.-S.; Chang, Y.-T. Imaging inflammation using an activated macrophage probe with Slc18b1 as the activation-selective gating target. *Nature Communications* **2019**, *10*, 1111.
13. Adachi, M.; Sugimoto, H.; Nishimura, Y.; Morita, K.; Ogino, C.; Fujii, M. Fluorophore-decorated Mie resonant silicon nanosphere for scattering/fluorescence dual-mode imaging. *Small* **2023**, 2207318.
14. Andersen, C. M.; Mortensen, G. Fluorescence spectroscopy: a rapid tool for analyzing dairy products. *Journal of Agricultural and Food Chemistry* **2008**, *56*, 720–729.
15. Lu, C.; Zhang, P.; Chen, S.; Zhu, J.; Xu, X.; Huang, H. Fluorescence spectrum photo-bleaching analysis for distinguishing microorganisms (bacteria and fungi) from other particles in air. *Optics Express* **2018**, *26*, 28902–28917.
16. Schmidt, T. D.; Lampe, T.; Sylvinson M. R., D.; Djurovich, P. I.; Thompson, M. E.; Brütting, W. Emitter orientation as a key parameter in organic light-emitting diodes. *Physical Review Applied* **2017**, *8*, 037001.

17. Yang, Y.; Zheng, Y.; Cao, W.; Titov, A.; Hyvonen, J.; Manders, J. R.; Xue, J.; Holloway, P. H.; Qian, L. High-efficiency light-emitting devices based on quantum dots with tailored nanostructures. *Nature Photonics* **2015**, *9*, 259–266.
18. Reimer, M. E.; Cher, C. The quest for a perfect single-photon source. *Nature Photonics* **2019**, *13*, 734–736.
19. Xu, L.; Yuan, H.; Zhang, N.; Zhang, J.; Bian, G.; Fan, P.; Li, M.; Zhang, C.; Zhai, Y.; Fang, J. High-efficiency fluorescence collection for NV- center ensembles in diamond. *Optics Express* **2019**, *27*, 10787–10797.
20. Sun, S.; Wu, L.; Bai, P.; Png, C. E. Fluorescence enhancement in visible light: dielectric or noble metal? *Physical Chemistry Chemical Physics* **2016**, *18*, 19324–19335.
21. Stamatopoulou, P. E.; Tserkezis, C. Role of emitter position and orientation on silicon nanoparticle-enhanced fluorescence. *OSA Continuum* **2021**, *4*, 918–932.
22. Geddes, C.; Lakowicz, J. Metal-enhanced fluorescence. *Journal of Fluorescence* **2002**, *12*, 121–129.
23. Hoang, T. B.; Akselrod, G. M.; Argyropoulos, C.; Huang, J.; Smith, D. R.; Mikkelsen, M. H. Ultrafast spontaneous emission source using plasmonic nanoantennas. *Nature Communications* **2015**, *6*, 7788.
24. Traverso, A. J.; Huang, J.; Peyronel, T.; Yang, G.; Tiecke, T. G.; Mikkelsen, M. H. Low-loss, centimeter-scale plasmonic metasurface for ultrafast optoelectronics. *Optica* **2021**, *8*, 202–207.
25. Doiron, B.; Mota, M.; Wells, M. P.; Bower, R.; Mihai, A.; Li, Y.; Cohen, L. F.; Alford, N. M.; Petrov, P. K.; Oulton, R. F.; Maier, S. A. Quantifying figures of merit for localized surface plasmon resonance applications: A materials survey. *ACS Photonics* **2019**, *6*, 240–259.

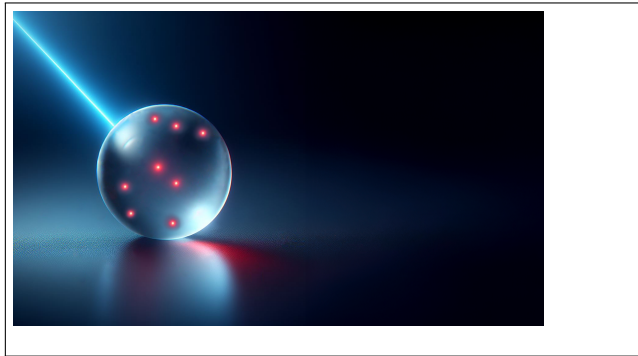
26. Sarychev, A. K.; Ivanov, A. V.; Barbillon, G. Limit possible electric field in plasmon nanogap resonator. **2021**, 2111.05511. *arXiv*. <https://arxiv.org/abs/2111.05511> (accessed Dec 14, 2023)
27. Mie, G. Beiträge zur Optik trüber Medien, speziell kolloidaler Metallösungen. *Annalen der Physik* **1908**, 330, 377–445.
28. Luk'yanchuk, B. S.; Bekirov, A. R.; Wang, Z. B.; Minin, I. V.; Minin, O. V.; Fedyanin, A. A. Optical Phenomena in Dielectric Spheres Several Light Wavelengths in Size: A Review. *Physics of Wave Phenomena* **2022**, 30, 217–241.
29. Wang, Z.; Luk'yanchuk, B.; Wu, B.; Yan, B.; Assel, A.; Yaminsky, I.; Yu, H.; Liu, L. Optical super-resonances in dielectric microsphere particles. *Proc. of SPIE*. 2022; p 1215205.
30. Rasskazov, I. L.; Carney, P. S.; Moroz, A. STRATIFY: a comprehensive and versatile MATLAB code for a multilayered sphere. *OSA Continuum* **2020**, 3, 2290–2309.
31. Ruppin, R. Decay of an excited molecule near a small metal sphere. *Journal of Chemical Physics* **1982**, 76, 1681–1684.
32. Ford, G.; Weber, W. Electromagnetic interactions of molecules with metal surfaces. *Physics Reports* **1984**, 113, 195–287.
33. Chew, H. Transition rates of atoms near spherical surfaces. *Journal of Chemical Physics* **1987**, 87, 1355–1360.
34. Chew, H. Radiation and lifetimes of atoms inside dielectric particles. *Physical Review A* **1988**, 38, 3410–3416.
35. Kim, Y. S.; Leung, P.; George, T. F. Classical decay rates for molecules in the presence of a spherical surface: A complete treatment. *Surface Science* **1988**, 195, 1–14.
36. Moroz, A. A recursive transfer-matrix solution for a dipole radiating inside and outside a stratified sphere. *Ann. Phys. (NY)* **2005**, 315, 352–418.

37. Bharadwaj, P.; Novotny, L. Spectral dependence of single molecule fluorescence enhancement. *Optics Express* **2007**, *15*, 14266–14274.
38. Sun, S.; Zhang, T.; Liu, Q.; Ma, L.; Du, Q.; Duan, H. Enhanced directional fluorescence emission of randomly oriented emitters via a metal-dielectric hybrid nanoantenna. *Journal of Physical Chemistry C* **2019**, *123*, 21150–21160.
39. Anger, P.; Bharadwaj, P.; Novotny, L. Enhancement and quenching of single-molecule fluorescence. *Physical Review Letters* **2006**, *96*, 113002.
40. Ringler, M.; Schwemer, A.; Wunderlich, M.; Nichtl, A.; Kürzinger, K.; Klar, T. A.; Feldmann, J. Shaping emission spectra of fluorescent molecules with single plasmonic nanoresonators. *Physical Review Letters* **2008**, *100*, 203002.
41. Arruda, T. J.; Bachelard, R.; Weiner, J.; Slama, S.; Courteille, P. W. Fano resonances and fluorescence enhancement of a dipole emitter near a plasmonic nanoshell. *Physical Review A* **2017**, *96*, 043869.
42. Sun, S.; Li, M.; Du, Q.; Png, C. E.; Bai, P. Metal-dielectric hybrid dimer nanoantenna: coupling between surface plasmons and dielectric resonances for fluorescence enhancement. *Journal of Physical Chemistry C* **2017**, *121*, 12871–12884.
43. Sun, S.; Rasskazov, I. L.; Carney, P. S.; Zhang, T.; Moroz, A. Critical role of shell in enhanced fluorescence of metal-dielectric core-shell nanoparticles. *Journal of Physical Chemistry C* **2020**, *124*, 13365–13373.
44. Rasskazov, I. L.; Moroz, A.; Carney, P. S. Electromagnetic energy in multilayered spherical particles. *Journal of the Optical Society of America A* **2019**, *36*, 1591–1601.
45. van Blaaderen, A.; Vrij, A. Synthesis and characterization of colloidal dispersions of fluorescent, monodisperse silica spheres. *Langmuir* **1992**, *8*, 2921–2931.

46. Gritsch, A.; Weiss, L.; Früh, J.; Rinner, S.; Reiserer, A. Narrow optical transitions in erbium-implanted silicon waveguides. *Physical Review X* **2022**, *12*, 041009.
47. Dulkeith, E.; Ringler, M.; Klar, T. A.; Feldmann, J.; Muñoz Javier, A.; Parak, W. J. Gold nanoparticles quench fluorescence by phase induced radiative rate suppression. *Nano Letters* **2005**, *5*, 585–589.
48. Acuna, G. P.; Bucher, M.; Stein, I. H.; Steinhauer, C.; Kuzyk, A.; Holzmeister, P.; Schreiber, R.; Moroz, A.; Stefani, F. D.; Liedl, T.; Simmel, F. C.; Tinnefeld, P. Distance dependence of single-fluorophore quenching by gold nanoparticles studied on DNA origami. *ACS Nano* **2012**, *6*, 3189–3195.
49. Rasskazov, I. L.; Moroz, A.; Carney, P. S. Extraordinary fluorescence enhancement in metal-dielectric core-shell nanoparticles. *Journal of Physical Chemistry Letters* **2021**, *12*, 6425–6430.
50. Rasskazov, I. L.; Moroz, A. Is there a proper figure of merit for a plasmonic structure involved in metal-enhanced fluorescence? *Plasmonics* **2022**, *17*, 1091–1094.
51. Lakowicz, J. R.; Shen, Y.; D’Auria, S.; Malicka, J.; Fang, J.; Gryczynski, Z.; Gryczynski, I. Radiative Decay Engineering. *Analytical Biochemistry* **2002**, *301*, 261–277.
52. de Vries, P.; Lagendijk, A. Resonant scattering and spontaneous emission in dielectrics: Microscopic derivation of local-field effects. *Physical Review Letters* **1998**, *81*, 1381–1384.
53. Harrington, R. On the gain and beamwidth of directional antennas. *IRE Transactions on Antennas and Propagation* **1958**, *6*, 219–225.
54. Chu, L. J. Physical limitations of omni-directional antennas. *Journal of Applied Physics* **1948**, *19*, 1163–1175.

55. Kinkhabwala, A.; Yu, Z.; Fan, S.; Avlasevich, Y.; Müllen, K.; Moerner, W. E. Large single-molecule fluorescence enhancements produced by a bowtie nanoantenna. *Nature Photonics* **2009**, *3*, 654–657.
56. Tovmachenko, O. G.; Graf, C.; van den Heuvel, D. J.; van Blaaderen, A.; Gerritsen, H. C. Fluorescence enhancement by metal-core/silica-shell nanoparticles. *Advanced Materials* **2006**, *18*, 91–95.
57. Ayala-Orozco, C.; Liu, J. G.; Knight, M. W.; Wang, Y.; Day, J. K.; Nordlander, P.; Halas, N. J. Fluorescence enhancement of molecules inside a gold nanomatryoshka. *Nano Letters* **2014**, *14*, 2926–2933.
58. Drexhage, K. H. In *Dye Lasers*; Schäfer, F. P., Ed.; Springer Berlin Heidelberg: Berlin, Heidelberg, 1973; Vol. 1; pp 144–193.
59. Drexhage, K. H. *Progress in Optics*; Elsevier, 1974; Vol. 12; pp 163–232.
60. de Dood, M. J. A.; Slooff, L. H.; Polman, A.; Moroz, A.; van Blaaderen, A. Modified spontaneous emission in erbium-doped SiO₂ spherical colloids. *Applied Physics Letters* **2001**, *79*, 3585–3587.
61. Rasskazov, I. L. <https://gitlab.com/iliarasskazov/stratify>. (accessed Dec 14, 2023) .
62. Bott, A.; Zdunkowski, W. Electromagnetic energy within dielectric spheres. *Journal of the Optical Society of America A* **1987**, *4*, 1361–1365.

TOC Graphic



Supporting Information:

Large fluorescence enhancement via lossless all-dielectric spherical mesocavities

Vadim I. Zakomirnyi,^{*,†} Alexander Moroz,[‡] Rohit Bhargava,[¶] and Ilia L.
Rasskazov[§]

[†]*Beckman Institute for Advanced Science and Technology, University of Illinois at
Urbana-Champaign, Urbana, IL 61801, USA*

[‡]*Wave-scattering.com*

[¶]*Departments of Bioengineering, Electrical & Computer Engineering, Mechanical Science
& Engineering, Chemical and Biomolecular Engineering and Chemistry, Cancer Center at
Illinois, Beckman Institute for Advanced Science and Technology, University of Illinois at
Urbana-Champaign, Urbana, IL 61801, USA*

[§]*SunDensity Inc., Rochester, NY 14604, USA*

E-mail: vazak@illinois.edu

Averaged fluorescence enhancement

The excitation rate γ_{exc} is governed by the electric dipole interaction term in the Hamiltonian $\sim \mathbf{E} \cdot \mathbf{d}$. The rate itself is proportional to $\sim |\mathbf{E} \cdot \mathbf{d}|^2$. At any given radial position, the averaging over all possible dipole orientations, while maintaining dipole magnitude, yields $\sim E_i E_j \overline{d_i d_j}$, where the summation over repeated indices is assumed. For unequal indices, $i \neq j$, to any $d_i d_j$ there corresponds another $d_i d_j$ with equal magnitude but opposite sign. Therefore upon averaging over all possible dipole orientations at a given radial position $E_i E_j \overline{d_i d_j}$ reduces to $E_j^2 \overline{d_j^2}$. But the averaged components $\overline{d_j^2}$ are all the same and equal to $\frac{1}{3}|\mathbf{d}|^2$. Thus at the end $E_j^2 \overline{d_j^2}$ reduces to $\frac{1}{3}|\mathbf{E}|^2 |\mathbf{d}|^2$. Ensuing averaging over all possible radial orientations, which is averaging over spherical shell of fixed radius r , affects only $|\mathbf{E}|^2$ but not $|\mathbf{d}|^2$. This ensures the decoupling of \mathbf{E} and \mathbf{d} in the averaging. When forming normalized dimensionless quantities, i.e. $\tilde{\gamma}_{exc}$ as the ratio of γ_{exc} with and without a sphere, the above factor $\frac{1}{3}|\mathbf{d}|^2$ cancels out, because it is the very same in the respective cases. Consequently, $\tilde{\gamma}_{exc}$ is entirely determined by the enhancement of the averaged electric intensity.

In a typical device (e.g. fluorescence probes for confocal imaging, tagging and tracing of organic molecules, etc) there is always a finite distribution of fluorescence emitters. Dipole moments of the emitters are as a rule also distributed randomly (e.g. ion beam implantation of rare earth emitters). Therefore, as far as devices are concerned, there are the averaged quantities which are relevant for their description. The averaging provides a relevant figure of merit in order to assess the fluorescence of a system under consideration. It is obvious that higher fluorescence enhancement can be achieved in practice by exercising a control over fluorophore dipole orientation and by judicious positioning of a fluorophore in suitable hot spots.

Local field corrections

The local field within the cavity, \mathbf{E}_{loc} , differs from an applied macroscopic field, \mathbf{E} by a local-field correction factor L , $\mathbf{E}_{loc} = L\mathbf{E}$. Local field corrections inside dielectrics exhibit the well-known (i) *real*, or *empty-cavity*, and (ii) *virtual-cavity*, or *Lorentz local-field*, factors for *substitutional* and *interstitial* atoms, respectively.^{S1}

The real cavity model assumes that (i) the atom is at the center of the cavity and (ii) the cavity itself has no other material, i.e. it is empty. The resulting ratio of local and macroscopic fields is given by [cf. electrostatic result (SI.3) below]

$$1 < L_{rc} = \frac{3\varepsilon}{2\varepsilon + 1} < \frac{3}{2}. \quad (\text{SI.1})$$

The substitutional case occurs prevalently for impurity atoms^{S1} and rare-earth emitters embedded within different organic complexes,^{S2} whenever the emitter embedded in a dielectric host expels the dielectric media and creates there a real tiny cavity. As pointed out by Böttcher based on the initial work of Onsager in 1933, the local-field correction factor depends also on the polarizability χ of the molecule placed in the cavity. The real cavity model applies when the polarizability of the guest dipole is sufficiently low compared to that of the host so that the reaction field caused by the induced dipole acting on the cavity can be neglected.^{S3}

The *virtual* cavity model assumes a uniform distribution of material within and outside the cavity.^{S1,S3-S5} The corresponding local-field correction is then known as the Lorentz local-field correction, eq 3,

$$1 < L_{vc} = \frac{\varepsilon + 2}{3}. \quad (\text{SI.2})$$

For pure systems constituted of only one kind of atom, or when the polarizability of the guest is the same as that of the host, the interstitial case of Ref.^{S1} described by the virtual-cavity model applies. This is also the case of rare earth emitters implanted in dielectrics by ion beam deposition.^{S6}

One can notice a significant difference between the respective local-field corrections (SI.1) and eq 3: whereas L_{rc} is strictly bounded by 3/2 from above, the Lorentz local-field correction (SI.2) increases indefinitely with increasing ε and is, in principle, unbounded from above. In general, L_{rc} represents a lower bound for the local field factor.^{S3}

The textbook derivation of local-field corrections is usually performed within quasi-static approximation.^{S1,S3-S5} Let us consider a sphere with dielectric constant ε_s embedded in a host characterized by dielectric constant ε_h . Irrespective of the units used, one finds for the sphere in the electrostatic case

$$\mathbf{E}_{loc} = \frac{3\varepsilon_h}{\varepsilon_s + 2\varepsilon_h} \mathbf{E}_{inc}. \quad (\text{SI.3})$$

The above familiar electrostatic result illustrates the necessity of applying local field corrections when estimating the local excitation field \mathbf{E}_{loc} felt inside a *real* cavity by atoms and molecules in the presence of a macroscopic field \mathbf{E}_{inc} .

Less known is a general derivation of the Lorentz local-field correction directly from the Maxwell's equations. In general, i.e. beyond the electrostatic approximation, the origin of the local-field factors is that the conventional electric dyadic Green's function is *not* sufficient to determine the correct value of $\mathbf{E}(\mathbf{r})$ at source points.^{S7} One has

$$\mathbf{E}(\mathbf{r}) = i\omega\mu_0 \lim_{\delta \rightarrow 0} \int_{V_j - V_\delta} \mathbf{G}(\mathbf{r}, \mathbf{r}') \cdot \mathbf{J}(\mathbf{r}') dV' + \frac{\mathbf{L} \cdot \mathbf{J}(\mathbf{r})}{i\omega\varepsilon_0}, \quad (\text{SI.4})$$

where V_δ is an excluded volume, i.e. a cavity comprising the observation point \mathbf{r} , \mathbf{G} is the Green's function to the equation

$$[\nabla \times \nabla \times - k^2] \mathbf{G} = \delta(\mathbf{r} - \mathbf{r}') \mathbf{I}, \quad (\text{SI.5})$$

and \mathbf{L} is an extra dyadics^{S7}

$$\mathbf{L} = \frac{1}{4\pi} \oint_{S_\delta} \frac{\mathbf{n} \otimes \mathbf{E}_{R'}}{R'^2} dS'. \quad (\text{SI.6})$$

Here \mathbf{n} is the unit normal pointing out of the principal volume and $\mathbf{E}_{R'}$ is the unit vector

pointing from \mathbf{r} to \mathbf{r}' . The integral on the rhs of (SI.4) is an *improper* nonconvergent integral in the sense of Kellogg,^{S8} i.e. it is necessary to restrict the shape of V_δ in order to obtain a limit when $V_\delta \rightarrow 0$. Nevertheless, although each of the two contributions on the rhs of (SI.4) does individually depend on the shape of excluded volume V_δ , the rhs of (SI.4) as a whole is independent of the shape of V_δ . For arbitrary principal volumes and time harmonic fields, \mathbf{L} can be concisely interpreted physically as a generalized depolarizing dyadics yielding the “local field” $\mathbf{E}_0 + \mathbf{L} \cdot \mathbf{J}/\varepsilon_0$ of electrostatics. Conversely, the depolarizing factors for an ellipsoid and the generalization to arbitrary shaped holes in or bodies of uniform volume sources can be found by the formula (SI.6).

Suppose one were to measure the electric field at a point within an enforced current distribution by removing an infinitesimally small volume V_δ of current and inserting an ideal point probe therein. Then the \mathbf{L} term determines the perturbation in electric field caused by the hypothetical measurement scheme of removing an infinitesimally small volume V_δ of enforced uniform current. Indeed, the measured field would then be given by (SI.4) but without the \mathbf{L} term, since the enforced current at this point has been removed. The measured local field would then be^{S7}

$$\mathbf{E}(\mathbf{r}) - \frac{\mathbf{L} \cdot \mathbf{J}}{i\omega\varepsilon_0}, \quad (\text{SI.7})$$

and would depend upon the shape of the infinitesimal volume and its relative position and orientation with respect to the point probe. Provided that \mathbf{J} here is merely an enforced polarization current, and assuming harmonic $e^{-i\omega t}$ time dependence,

$$\mathbf{J} = \partial_t \mathbf{P} = -i\omega \mathbf{P}, \quad (\text{SI.8})$$

one obtains in the case of dielectrics

$$\mathbf{J}(\mathbf{r}) = -i\omega\varepsilon_0(\varepsilon(\mathbf{r}) - 1)\mathbf{E}(\mathbf{r}), \quad (\text{SI.9})$$

where ε is the relative dielectric contrast, $\varepsilon(\mathbf{r}) = \varepsilon(\mathbf{r})/\varepsilon_h$. The extra dyadics is known for a variety of different principal volumes. For instance, $\mathbf{L} = \mathbf{I}/3$ for a *sphere* and a *cube* (see Table 1 in Ref.^{S7}). According to (SI.7)-(SI.9), the measured local field is then

$$\mathbf{E}_{loc}(\mathbf{r}) = \mathbf{E}(\mathbf{r}) + \frac{\mathbf{P}}{3\varepsilon_0} = \mathbf{E}(\mathbf{r}) \left(1 + \frac{\varepsilon(\mathbf{r}) - 1}{3} \right) = \frac{\varepsilon(\mathbf{r}) + 2}{3} \mathbf{E}(\mathbf{r}). \quad (\text{SI.10})$$

This way the quasi-static Lorentz factor, or the Lorentz local-field correction in eq 3, is recovered.

References

- (S1) de Vries, P.; Legendijk, A. Resonant scattering and spontaneous emission in dielectrics: Microscopic derivation of local-field effects. *Physical Review Letters* **1998**, *81*, 1381–1384.
- (S2) Duan, C.-K.; Reid, M. F.; Wang, Z. Local field effects on the radiative lifetime of emitters in surrounding media: Virtual- or real-cavity model? *Physics Letters A* **2005**, *343*, 474–480.
- (S3) Aubret, A.; Orrit, M.; Kulzer, F. Understanding local-field correction factors in the framework of the Onsager-Böttcher model. *ChemPhysChem* **2019**, *20*, 345–355.
- (S4) Aspnes, D. E. Local-field effects and effective-medium theory: A microscopic perspective. *American Journal of Physics* **1982**, *50*, 704–709.
- (S5) Dolgaleva, K.; Boyd, R. W. Local-field effects in nanostructured photonic materials. *Advances in Optics and Photonics* **2012**, *4*, 1–77.
- (S6) de Dood, M. J. A.; Slooff, L. H.; Polman, A.; Moroz, A.; van Blaaderen, A. Local optical density of states in SiO₂ spherical microcavities: Theory and experiment. *Physical Review A* **2001**, *64*, 033807.

- (S7) Yaghjian, A. Electric dyadic Green's functions in the source region. *Proceedings of the IEEE* **1980**, 68, 248–263.
- (S8) Kellogg, O. D. *Foundations of Potential Theory*; Springer Berlin Heidelberg: Berlin, Heidelberg, 1967.